Fulde-Ferrell-Larkin-Ovchinnikov state to topological superfluidity transition in bilayer spin-orbit-coupled degenerate Fermi gases

Liang-Liang Wang,[1] Qing Sun,[2,*] W.-M. Liu,[1] G. Juzeliūnas,[3,†] and An-Chun Ji[2,‡]

[1]*Beijing National Laboratory for Condensed Matter Physics, Institute of Physics, Chinese Academy of Sciences, Beijing 100190, China*

[2]*Department of Physics, Capital Normal University, Beijing 100048, China*

[3]*Institute of Theoretical Physics and Astronomy, Vilnius University, A. Goštauto 12, Vilnius 01108, Lithuania*

(Received 14 February 2017; published 24 May 2017)

Recently a scheme has been proposed for generating the two-dimensional Rashba-type spin-orbit coupling (SOC) for ultracold atomic bosons in a bilayer geometry [S.-W. Su *et al.*, Phys. Rev. A **93**, 053630 (2016)]. Here we investigate the superfluidity properties of a degenerate Fermi gas affected by the SOC in such a bilayer system. We demonstrate that a Fulde-Ferrell-Larkin-Ovchinnikov (FFLO) state appears in the regime of small to moderate atom-light coupling. In contrast to the ordinary SOC, the FFLO state emerges in the bilayer system without adding any external fields or spin polarization. As the atom-light coupling increases, the system can transit from the FFLO state to a topological superfluid state. These findings are also confirmed by the Bogoliubov—de Gennes simulations with a weak harmonic trap added.

DOI: 10.1103/PhysRevA.95.053628

I. INTRODUCTION

The search for new exotic quantum states [1,2] is a fundamental issue in current condensed-matter physics. This topic has drawn enormous interest for ultracold atomic gases [3–8], enabling simulations of many condensed-matter phenomena. With recent experimental progress in synthetic spin-orbit coupling (SOC) for degenerate atomic gases [9–17], diverse new quantum phases due to the SOC have been predicted [7,18,19], such as the stripe phase and vortex structure in the ground states of atomic Bose-Einstein condensates (BECs) [20–31], as well as the Rashba pairing bound states (Rashbons) [32,33] and topological superfluidity [34–38] in degenerate Fermi gases.

The synthetic SOC has been successfully implemented and explored by Raman coupling of a pair of atomic hyperfine ground states accompanied by a recoil [9–13]. This provides the SOC along the recoil direction representing the one-dimensional (1D) SOC. The realization of the synthetic SOC for ultracold atoms in two or more dimensions is very desirable. The two-dimensional (2D) SOC of the Rashba type has a nontrivial dispersion. The lower dispersion branch contains a highly degenerate ground state (the Rashba ring). Additionally, there is a Dirac cone at an intersection point of two dispersion branches, and a band gap can be opened by adding a Zeeman term. This is essential for the topological superfluidity. Recently, a number of elaborate schemes has been suggested to create an effective 2D and three-dimensional (3D) SOC [39–52]. Subsequently the 2D SOC has been experimentally implemented [14–16] by inducing the Raman transitions between three atomic hyperfine ground states in a ring coupling scheme [14,15,45], as well as by using another approach which relies on optical lattices [16,50]. However, in the experiments [14,15] one of the three atomic states belongs to a higher hyperfine manifold leading to losses.

Recently Su *et al.* [52] put forward a scheme for generating the effective Rashba SOC for a two-component atomic BEC confined in a bilayer geometry. The layer index provides an extra degree of freedom to form a basis of four combined spin-layer states composed of two spin and two layer states. The four spin-layer states are coupled in a cyclic manner by means of the spin-flip Raman transitions [9] and the laser-assisted interlay coupling [53–57], both processes being accompanied by recoil. This provides effectively a ring coupling scheme [52] leading to the Rashba-type SOC. In contrast to the original ring coupling scheme [45] involving four atomic internal states, the bilayer setup makes use of only two atomic spin states [52], like the NIST scheme for the 1D SOC [9]. Hence there is no need to employ spin states belonging to a higher hyperfine manifold which suffers from a collisional population decay undermining the effective SOC. Therefore, the bilayer scheme offers a more feasible system to study the many-body physics due to 2D SOC.

Topological superfluidity has attracted an enormous interest in SO coupled fermion gases [34–38,58–62]. These works considered a pure 2D or 3D Rashba-type SOC for ultracold atoms with two internal (spin up and down) states. However, in a realistic atomic system the SOC is produced in an effective manner by laser dressing of a number of atomic internal states and restricting atomic motion to a manifold of two-fold degenerate dressed states. As a result, the topological superfluidity is more involved, an issue which has been little investigated.

Here, we explore the topological superfluidity of a Fermi gas affected by the SOC. The SOC is produced using the bilayer scheme previously considered for bosonic atoms [52,63]. A characteristic feature of the bilayer system is that the interaction takes place mostly between atoms belonging to the same layer [52]. Therefore the atom-atom interactions differ considerably from the ones featured in the SOC scheme involving four cyclically coupled atomic internal states [45]. In the latter situation the atoms in all four internal states interact with approximately the same strength.

We find that the bilayer scheme provides an intriguing phase transition of superfluidity. In the regimes of small and moderate

*sunqing@cnu.edu.cn

†gediminas.juzeliunas@tfai.vu.lt

‡andrewjee@sina.com

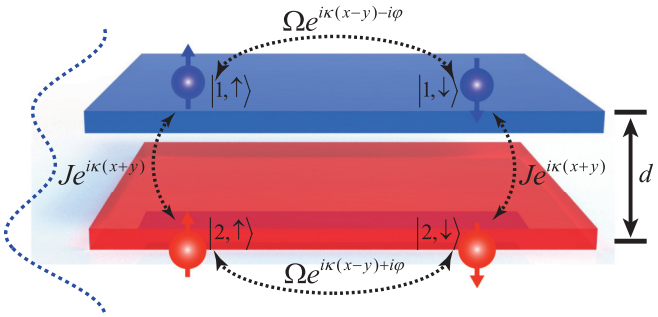

FIG. 1. Schematic representation of a Fermi gas in a bilayer structure. An asymmetric double-well potential along the z axis traps the atoms in two layers separated by a distance d. The combined spin-layer atomic states $|j=1,2,\gamma=\uparrow,\downarrow\rangle$ are cyclically coupled by the intralayer Raman transitions and interlayer laser-assisted tunneling characterized by the matrix elements $\Omega e^{i\kappa(x-y)\pm i\varphi}$ and $Je^{i\kappa(x+y)}$, respectively.

atom-light coupling the FFLO states emerge. The FFLO states involve pairing with a finite center-of-mass momentum. These states have received a considerable attention in different physical contexts [64–69]. In general, the FFLO state arises in the spin-polarized systems or can be induced by in-plane Zeeman fields in the SO coupled Fermi gases [67,68]. Here we show that for the small to moderate atom-light coupling the FFLO states emerge intrinsically in the bilayer system without any external magnetic field or spin polarization. As the atom-light coupling increases, the system can undergo a transition from the FFLO state to the topological superfluid (TS). The TSs have been pursued theoretically in model Hamiltonians with the 2D (3D) Rashba-type SOC [34–38,58–62]. Here we provide convincing evidences that TSs can also occur in the experimentally feasible bilayer system.

II. MODEL AND SINGLE-PARTICLE SPECTRUM

We consider a two-component Fermi gas confined in the bilayer geometry as illustrated in Fig. 1. The atoms are confined in a deep enough asymmetric double-well potential [70], so their motion in the z direction is restricted to the ground states of individual wells separated by a distance d. On the other hand, the laser-assisted tunneling can induce transitions between the two wells.

The system is described by four combined spin-layer states $|j,\gamma\rangle = |j\rangle_{\text{layer}} \otimes |\gamma\rangle_{\text{spin}}$ which serve as the states required for the ring coupling scheme [45]. Here $j=1,2$ signifies the jth layer, and $\gamma=\uparrow,\downarrow$ denotes an internal atomic state. For example, the states with $\gamma=\uparrow,\downarrow$ can be the $m_F=9/2$ and $m_F=7/2$ magnetic sublevels of the $F=9/2$ hyperfine ground-state manifold of fermion ^{40}K atoms, like in the experiment [11] on the 1D SOC.

The four atomic states $|j,\gamma\rangle$ are coupled in a cyclic manner via the spin-flip Raman transitions and the interlayer laser-assisted tunneling characterized by the matrix elements $\Omega(\mathbf{r}) = \Omega e^{i\kappa(x-y)\pm i\varphi}$ and $J(\mathbf{r}) = Je^{i\kappa(x+y)}$, respectively. As discussed in Ref. [52], such Raman transitions and interlayer tunneling can be induced using three properly chosen laser beams. The Raman coupling provides a recoil in the $x+y$ direction, whereas the interlayer tunneling is accompanied by a recoil in the $x-y$ direction. Here $\kappa\sqrt{2}$ is a magnitude of the in-plane momentum transferred by the lasers, and $2\varphi = k_z d$ is a phase difference of the Raman coupling between the two layers due to an out-of-plane recoil momentum k_z [52].

The recoil momentum k_z can also influence the atomic center-of-mass motion in the z direction. However, the latter effect is not important if the atoms are confined strongly by the potential wells in the z direction. This is justifiable if the depth of each well comprising the asymmetric double-well potential exceeds considerably the recoil energy. Consequently in each layer the atomic ground state is localized in the z direction over distances much smaller than the wavelength $\lambda_z = 2\pi/k_z$ corresponding to the atomic recoil accompanying the spin-flip transitions. In that case, the atoms remain in the ground states of individual potential wells after spin-flip transitions.

A. Hamiltonian and system

Performing a gauge transformation eliminating the position dependence of the atom-light coupling matrix elements $\Omega(\mathbf{r})$ and $J(\mathbf{r})$, the bilayer system is described by the following Hamiltonian [71]:

$$\hat{H} = H_{\text{kin}} + H_{\text{Laser}} + H_{\text{SOC}} + H_{\text{int}}, \tag{1}$$

where

$$H_{\text{kin}} = \int d^2\mathbf{r}\Sigma_{j,\gamma}\hat{\psi}^\dagger_{j\gamma}\left[\frac{\hbar^2k^2}{2m} - \mu\right]\hat{\psi}_{j\gamma}, \tag{2}$$

$$H_{\text{Laser}} = \int d^2\mathbf{r}\Omega[e^{i\varphi}\hat{\psi}^\dagger_{1\uparrow}\hat{\psi}_{1\downarrow} + e^{-i\varphi}\hat{\psi}^\dagger_{2\uparrow}\hat{\psi}_{2\downarrow} + \text{H.c.}] + \int d^2\mathbf{r}\Sigma_\gamma J\hat{\psi}^\dagger_{2\gamma}\hat{\psi}_{1\gamma} + \text{H.c.}, \tag{3}$$

$$H_{\text{SOC}} = \int d^2\mathbf{r}\frac{\hbar^2\kappa}{m}[\hat{\psi}^\dagger_{2\uparrow}k_x\hat{\psi}_{2\uparrow} - \hat{\psi}^\dagger_{1\downarrow}k_x\hat{\psi}_{1\downarrow} + \hat{\psi}^\dagger_{2\downarrow}k_y\hat{\psi}_{2\downarrow} - \hat{\psi}^\dagger_{1\uparrow}k_y\hat{\psi}_{1\uparrow}],$$

$$H_{\text{int}} = -g\int d^2\mathbf{r}\sum_j\hat{\psi}^\dagger_{j\uparrow}\hat{\psi}^\dagger_{j\downarrow}\hat{\psi}_{j\downarrow}\hat{\psi}_{j\uparrow}, \tag{4}$$

where $\hat{\psi}_{j\gamma} \equiv \hat{\psi}_{j\gamma}(\mathbf{r})$ is a fermion field operator for annihilation of an atom positioned at $\mathbf{r}$ in a layer $j=1,2$ with a spin state $\gamma=\downarrow,\uparrow$. The first term H_{kin} represents the Hamiltonian for an unperturbed atomic motion within the layers, μ being the chemical potential. The second term H_{Laser} accommodates the spin-flip intralayer Raman transitions characterized by the Rabi frequency Ω, as well as the laser-assisted interlayer tunneling described by the strength J. The third term H_{SOC} represents the SOC due to the recoil momentum κ in the xy plane induced by the interlayer tunneling and Raman transitions [52]. The latter SOC term was not included in the previous analysis of the superfluidity for the fermions in a bilayer geometry [62].

As one can see in Fig. 1 and Eq. (3), the amplitude of the Raman coupling $\Omega e^{\pm i\varphi}$ contains a relative phase $2\varphi = k_z d$ between the upper and lower layers. The phase 2φ can be changed by either varying the double-well separation d or the out-of-plane Raman recoil momentum k_z. For $\varphi=\pi/2$ a Dirac cone appears in the single-particle spectrum of the

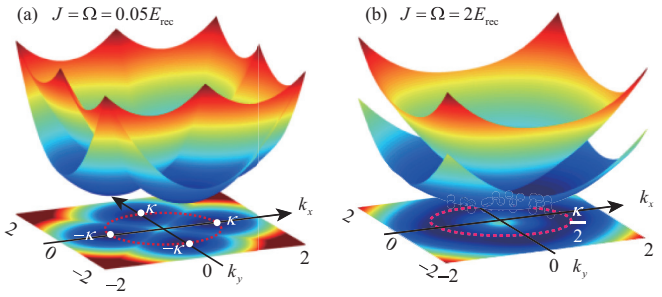

FIG. 2. Single-particle dispersion of the lowest two branches for various coupling strengths and $\varphi=\pi/2$. (a) In a weak coupling regime $\Omega=J\ll E_{\rm rec}$, the dispersion is a superimposition of four distinct paraboloids nearly centered at $(\pm\kappa,\pm\kappa)$. (b) In the strong coupling regime $\Omega=J\gg E_{\rm rec}$, the Rashba-ring minimum (red dashed line) with a radius $\kappa/2$ emerges.

ring coupling scheme [45,52]. A gap is opened in the Dirac spectrum for $\varphi\neq\pi/2$. This is important for formation of the topological superfluidity.

Finally, $H_{\rm int}$ describes the on-site attractive interaction ($g>0$) between atoms situated in the same layer. Here the bare s-wave interaction g is related to the binding energy E_b of the two-body bound state [72] via

$$1/g=\sum_{\mathbf{k}}1/(2\varepsilon_{\mathbf{k}}-E_b), \tag{5}$$

where $\varepsilon_{\mathbf{k}}=\hbar^2\mathbf{k}^2/(2m)$ is the kinetic energy. In experiments, the binding energy E_b can be tuned via the Feshbach resonance technique.

B. Effective single-particle Hamiltonian

We shall focus on a situation of a symmetric coupling: $\Omega=J$. Figure 2 plots the single-particle dispersion. If $\Omega=J\ll E_{\rm rec}$, the minima of the single-particle dispersive paraboloids appear at $(\pm\kappa,\pm\kappa)$, where $E_{\rm rec}=\hbar^2\kappa^2/2m$ is a characteristic energy of the in-plane recoil. The dispersion is then built of four distinct superimposed paraboloids, each corresponding to individual spin-layer states $|j,\gamma\rangle$. As the coupling increases (but $\Omega=J\leqslant E_{\rm rec}$), the four paraboloids gradually coalesce. Yet the dispersion still exhibits four distinguishable minima in the lowest branch. The locations of the four minima would gradually move toward the center $k=0$ as the coupling increases. Finally in the strong coupling regime, $\Omega=J\gg E_{\rm rec}$, the mixing between the spin states results in the emergence of a cylindrically symmetric Rashba-ring minimum of radius $\kappa/2$ [45,52]. In this case, one can project the Hamiltonian onto the lowest two energy states leading to the usual single-particle Hamiltonian of the Rashba type (see Appendix A)

$$H_{\rm eff}=\begin{pmatrix}\mathbf{k}^2/2m-\mu'-h_z & \alpha(k_y-ik_x)\\ \alpha(k_y+ik_x) & \mathbf{k}^2/2m-\mu'+h_z\end{pmatrix}, \tag{6}$$

where $\mu'=\mu-\Delta\mu$ is an effective chemical potential, $\alpha=\kappa/2m$, and $\Delta\mu=E_{\rm rec}-\Omega\sqrt{2}\cos(\delta\varphi/2)$. Here

$$h_z=\Omega\sqrt{2}\sin(\delta\varphi/2),\quad\text{with}\quad\delta\varphi=\varphi-\pi/2, \tag{7}$$

is an effective Zeeman field which is controlled by tuning the relative phase φ for the Raman coupling. For $\varphi=\pi/2$ we have $h_z=0$, leading to the usual Dirac cone at $k=0$. The Dirac cone is opened if the phase φ deviates from $\pi/2$.

III. ANALYSIS OF THE SUPERFLUIDITY

A. Method

By introducing the superfluid order parameters $\Delta_j(\mathbf{r})=g\langle\psi_{j,\downarrow}(\mathbf{r})\psi_{j,\uparrow}(\mathbf{r})\rangle$ with $\mathbf{r}=(x,y)$, the Hamiltonian (4) can be diagonalized via a Bogoliubov–Valatin transformation [73]. In doing so we have additionally included a weak harmonic trapping potential $V(r)=m\omega^2r^2/2$. The resultant Bogoliubov-de Gennes (BdG) equation

$$H_{\rm BdG}(\mathbf{r})\phi_\eta=\varepsilon_\eta\phi_\eta \tag{8}$$

is described by an 8×8 matrix Hamiltonian

$$H_{\rm BdG}(\mathbf{r})=\begin{pmatrix}H_1(\mathbf{r}) & \mathcal{J}\\ \mathcal{J}^\dagger & H_2(\mathbf{r})\end{pmatrix}, \tag{9}$$

where a diagonal 4×4 matrix $\mathcal{J}=\mathrm{diag}(J,J,-J,-J)$ describes the interlayer coupling, and $H_{1,2}(\mathbf{r})$ is a 4×4 matrix Hamiltonian for an uncoupled layer $j=1,2$:

$$H_1(\mathbf{r})=\begin{pmatrix}\epsilon_{1\uparrow}(\mathbf{r}) & \Omega e^{-i\varphi} & 0 & \Delta_1(\mathbf{r})\\ \Omega e^{i\varphi} & \epsilon_{1\downarrow}(\mathbf{r}) & -\Delta_1(\mathbf{r}) & 0\\ 0 & -\Delta_1^*(\mathbf{r}) & -\epsilon_{1\uparrow}^*(\mathbf{r}) & -\Omega e^{-i\varphi}\\ \Delta_1^*(\mathbf{r}) & 0 & -\Omega e^{i\varphi} & -\epsilon_{1\downarrow}^*(\mathbf{r})\end{pmatrix}, \tag{10}$$

and

$$H_2(\mathbf{r})=\begin{pmatrix}\epsilon_{2\uparrow}(\mathbf{r}) & \Omega e^{i\varphi} & 0 & \Delta_2(\mathbf{r})\\ \Omega e^{-i\varphi} & \epsilon_{2\downarrow}(\mathbf{r}) & -\Delta_2(\mathbf{r}) & 0\\ 0 & -\Delta_2^*(\mathbf{r}) & -\epsilon_{2\uparrow}^*(\mathbf{r}) & -\Omega e^{i\varphi}\\ \Delta_2^*(\mathbf{r}) & 0 & -\Omega e^{-i\varphi} & -\epsilon_{2\downarrow}^*(\mathbf{r})\end{pmatrix}, \tag{11}$$

with

$$\begin{aligned}\epsilon_{1\uparrow}(\mathbf{r})&=-\hbar^2\nabla^2/(2m)+i\hbar^2\kappa\partial_y/m+V(\mathbf{r})-\mu,\\ \epsilon_{1\downarrow}(\mathbf{r})&=-\hbar^2\nabla^2/(2m)+i\hbar^2\kappa\partial_x/m+V(\mathbf{r})-\mu,\\ \epsilon_{2\uparrow}(\mathbf{r})&=-\hbar^2\nabla^2/(2m)-i\hbar^2\kappa\partial_x/m+V(\mathbf{r})-\mu,\\ \epsilon_{2\downarrow}(\mathbf{r})&=-\hbar^2\nabla^2/(2m)-i\hbar^2\kappa\partial_y/m+V(\mathbf{r})-\mu,\end{aligned} \tag{12}$$

The Nambu basis is chosen as $\phi_\eta=[u_{1\uparrow,\eta},u_{1\downarrow,\eta},v_{1\uparrow,\eta},v_{1\downarrow,\eta},u_{2\uparrow,\eta},u_{2\downarrow,\eta},v_{2\uparrow,\eta},v_{2\downarrow,\eta}]^T$, and ε_η is the corresponding energy of Bogoliubov quasiparticles labeled by an index η. The order parameter $\Delta_{1,2}(\mathbf{r})$ is to be determined self-consistently by

$$\Delta_j(\mathbf{r})=g\sum_\eta[u_{j\uparrow,\eta}v_{j\downarrow,\eta}^*f(-\varepsilon_\eta)+u_{j\downarrow,\eta}v_{j\uparrow,\eta}^*f(\varepsilon_\eta)],$$

where $f(E)=1/[e^{E/k_BT}+1]$ is the Fermi-Dirac distribution function at a temperature T. The chemical potential μ is determined using the number equation $N=\int d\mathbf{r}\,n(\mathbf{r})$, where the total atomic density is given by

$$n(\mathbf{r})=\sum_{j\gamma,\eta}[|u_{j\gamma,\eta}(\mathbf{r})|^2f(\varepsilon_\eta)+|v_{j\gamma,\eta}(\mathbf{r})|^2f(-\varepsilon_\eta)]. \tag{13}$$

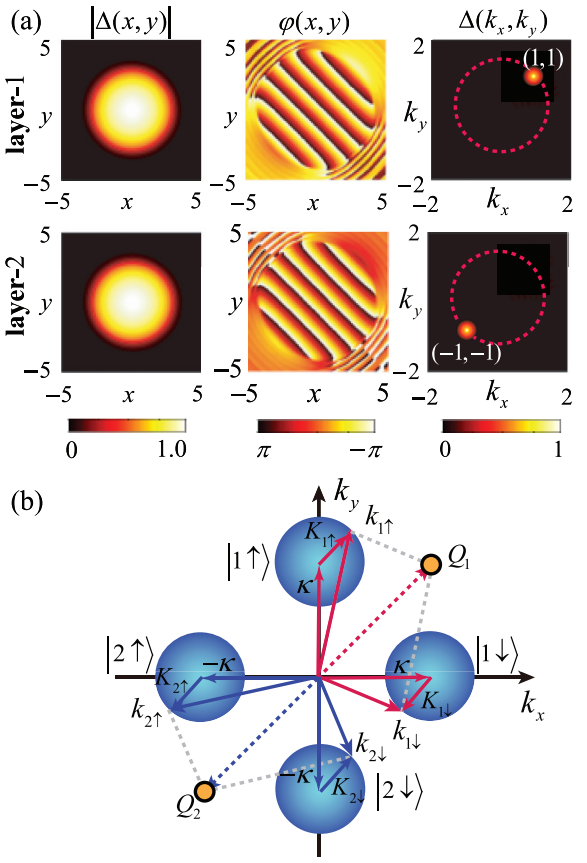

FIG. 3. (a) Real-space density profile (left panel) and phase configurations (middle panel) of the order parameters $\Delta_{1,2}$ for $\Omega = J = 0.05E_{\rm rec}$ and $\varphi = \pi/2$. Here we have taken $N_{\rm atom} = 100$ and $E_b = 2E_{\rm rec}$. The right panel shows the corresponding momentum-space distribution. (b) An illustration of the FFLO-type of the Cooper pairing mechanism. The red and blue solid arrows represent the Cooper pairing momenta of atoms in the first and second layers, with $\mathbf{Q}_{1,2}$ denoting the total paring momentum.

We have solved the BdG equation self-consistently by using the basis expansion method [61]. In the numerical simulations we take a large energy cutoff $\varepsilon_c = 6E_{\rm rec}$ to ensure the accuracy of the calculation, where $E_{\rm rec} = 10\hbar\omega$ assures the trap oscillation frequency is much smaller than the recoil frequency. Throughout this work we focus on the case of zero temperature. The temperature of the gas T is about $0.2 \sim 0.3T_{\rm F}$ for a total number of atoms $N_{\rm atom} = 100$ used in the calculations if one takes the Fermi temperature $T_{\rm F}$ to be around 300 nK [74]. Such a temperature T is sufficiently low, so the results of the calculation are almost unaffected by taking the zero temperature limit.

B. Results

We start with a weak coupling limit $\Omega = J \ll E_{\rm rec}$. Figure 3 plots the corresponding density profiles and phase configurations for the order parameter $\Delta_{1,2}(\mathbf{r})$. The fermions are assumed to populate only the lowest branch, so the Fermi surface forms four Fermi pockets centered at $(\pm\kappa, \pm\kappa)$. The first two points $(\kappa,0)$ and $(0,\kappa)$ correspond to the spin up and down states for the first layer, whereas the remaining two points $(-\kappa,0)$ and $(0,-\kappa)$ correspond to the spin up and down states for the second layer. Note that atoms prefer to pair in the same layer, since only the atoms situated in the same layer interact. We have found that the order parameters $\Delta_{1,2}(\mathbf{r}) = \Delta_0 e^{i\mathbf{Q}_{1,2}\cdot\mathbf{r}}$ exhibit an oscillating structure along the diagonal directions $\mathbf{Q}_1 = \kappa(\mathbf{e}_x + \mathbf{e}_y)$ and $\mathbf{Q}_2 = -\mathbf{Q}_1$, as shown in Fig. 3(a). This is a key feature of the so-called FFLO phase. In Fig. 3(b), we illustrate the underlying pairing mechanism of the FFLO state.

If we choose the first layer, the wave vectors for the two pockets $(\kappa,0)$ and $(0,\kappa)$ can be written as $\mathbf{k}_{1\uparrow} = \kappa\mathbf{e}_y + \mathbf{K}_{1\uparrow}$ and $\mathbf{k}_{1\downarrow} = \kappa\mathbf{e}_x + \mathbf{K}_{1\downarrow}$. Here $\mathbf{K}_{1\uparrow(\downarrow)}$ denotes the atomic momentum calculated with respect to the center of each Fermi pocket. When $\mathbf{K}_{1\uparrow} = -\mathbf{K}_{1\downarrow}$, fermions can pair together in different pockets with opposite momenta. In this case the total momentum $\mathbf{k}_{1\uparrow} + \mathbf{k}_{1\downarrow}$ of the atomic pair in the first layer reads $\mathbf{Q}_1 = \kappa(\mathbf{e}_x + \mathbf{e}_y)$. In a similar manner, the pairing center-of-mass of momentum is $\mathbf{Q}_2 = -\kappa(\mathbf{e}_x + \mathbf{e}_y)$ for the second layer, as one can see in Fig. 3(b).

As the coupling $\Omega = J$ increases, the four paraboloids are mixed by the intralayer spin-flip atomic transitions and interlayer tunneling. In that case the four Fermi surface pockets

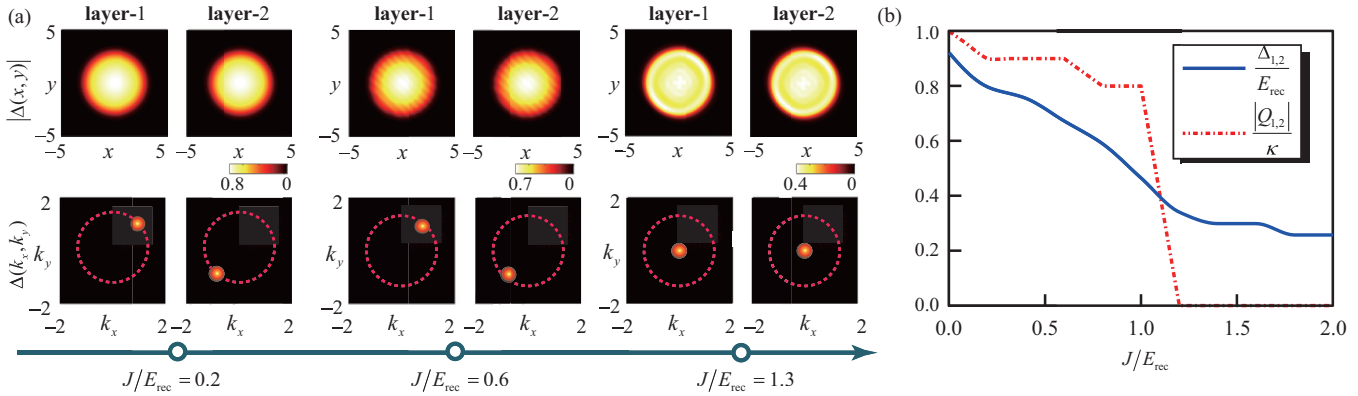

FIG. 4. (a) Profiles of the order parameter $\Delta(\mathbf{r})$ (up) and the corresponding momentum distributions (down) in the first and second layers for the $\Omega = J = 0.2, 0.6, 1.3E_{\rm rec}$. Other parameters are $E_b = 2E_{\rm rec}$, $\varphi = \pi/2$, and $N_{\rm atom} = 100$. (b) Evolution of the order parameter $\Delta_{1,2}$ (maximum of the order parameter in the whole region) (blue solid line) and the magnitude of the FFLO vector $|\mathbf{Q}_{1,2}|$ (red dashed-dotted line) are plotted as a function of the interlayer tunneling strength $J = \Omega$.

still remain, but the central locations of the pockets shrink toward the momentum center $k = 0$. In this case, the FFLO state sustains, but with the FFLO pairing amplitude Δ_0 being reduced. Figure 4 depicts the evolution of the order parameters $\Delta_{1,2}$ and corresponding momentum dispersions $Q_{1,2}$ for various coupling strengths. We see that the pairing momentum decreases as the coupling increases. Around $J \gtrsim E_{\rm rec}$, the four paraboloids begin to merge together, the atoms tend to pair with zero relative momentum, and the system enters a normal superfluid state.

Let us now investigate a feasibility of the topological superfluidity in the bilayer system for $\Omega = J$. For this purpose, we allow the relative phase of the Raman coupling φ to deviate from $\pi/2$, so $\delta\varphi = \varphi - \pi/2 \neq 0$. Consequently the energy gap $E(\delta\varphi) = 2h_z = 2\sqrt{2}\Omega\sin(\delta\varphi/2)$ appears in the single-particle spectrum at the Dirac point $\mathbf{k} = 0$ in the strong coupling (Rashba) regime. The phase diagram is illustrated in Fig. 5. As anticipated, at the strong coupling one can find a TS phase which is characterized by a nonzero Chern number $C = 1$ and a zero pairing momentum $Q = 0$. Here the Chern number is calculated by a self-consistent solution of the BdG equation (8) at the center of the trap where the changes in the trapping potential are minimum (see the Appendix B). As shown in Fig. 5, there is a phase transition from normal to topological superfluids when the chemical potential enters the energy gap. Moreover, the FFLO and NS states have also been identified by observing the states with $Q \neq 0$ and $Q = 0$, $C = 0$, respectively. For the moderate coupling, $\Omega = J < E_{\rm rec}$, the bilayer system stays in the FFLO state. Similar to the $\varphi = \pi/2$ case discussed above, such a FFLO state would undergo a transition to the NS when the coupling strength is increased to $J_{c1} \gtrsim E_{\rm rec}$. In the strong coupling regime, $\Omega = J \gtrsim 1.5E_{\rm rec}$, corresponding to the limit of the effective Rashba-type SOC, the system can be in a TS state if the chemical potential is situated within the energy gap $E(\delta\phi)$. Hence there exists another critical coupling strength J_{c2} for the transition between the NS and TS. In Fig. 5 the dashed blue and red solid lines indicate the phase transitions FFLO $\rightarrow$ NS and NS $\rightarrow$ TS, respectively. It is noteworthy that the critical coupling J_{c2} for the transition between the NS and TS states increases with the binding energy E_b because of the increase of the chemical potential.

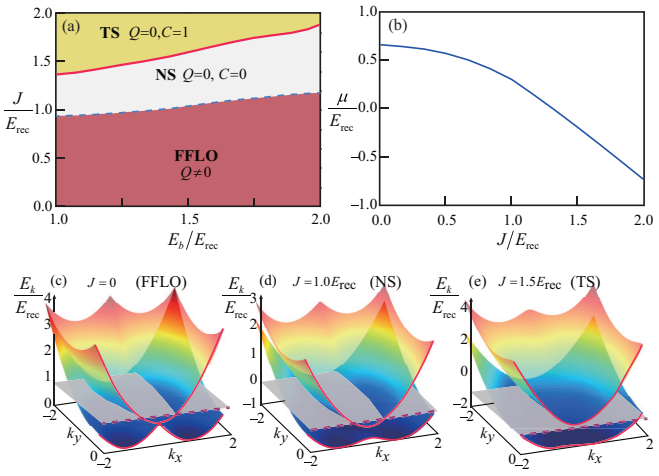

FIG. 5. Phases of the bilayer system for $\Omega = J$ and $\varphi = 0.6\pi$. (a) Phase diagram in the (E_b, J) plane for $N_{\rm atom} = 100$. Three phases are formed: a FFLO superfluid represented by a dark red region, a normal superfluid (NS, white region) and a topological superfluid (TS, yellow region). The latter phase is characterized by a nonzero Chern number C and a zero pairing momentum Q. (b) Chemical potential μ as a function of the interlayer tunneling J at the binding energy $E_b = 1.0E_{\rm rec}$. (c)–(e) Two lowest branches of the single-particle dispersion for different values of J corresponding to different phases. Here the chemical potential is represented by a gray plane. The dispersion branches become lower with an increase of J, leading to a decrease of the chemical potential, as one can see in (b)–(e). The NS phase transforms to the TS phase when the chemical potential enters the energy gap, as one can see comparing (d) and (e). In (c)–(e) the momentum is measured in the units of the recoil momentum κ.

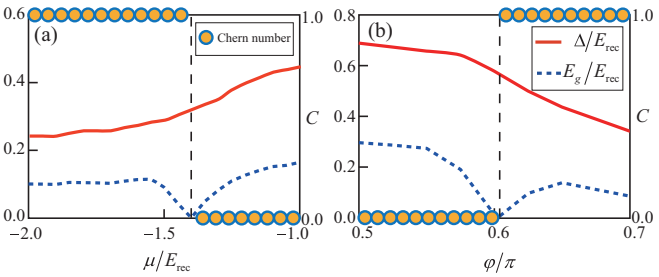

FIG. 6. Evolution of parameters of the system across the topological phase boundary. (a) Behavior of the minimum excitation gap $E_{\rm g}$ (blue dashed line) and the order parameter $\Delta_{1,2} = \Delta$ (red solid line) with increasing chemical potential for $E_b = 3E_{\rm rec}$, $J \equiv \Omega = 2E_{\rm rec}$, and $\varphi = 3/4\pi$. (b) Minimum excitation gap and pairing order parameter against the tunneling phase φ for $E_b = 3E_{\rm rec}$, $J \equiv \Omega = 2E_{\rm rec}$, and $\mu = -0.5E_{\rm rec}$. The yellow filled circles indicate the integer Chern number C which is a topological invariant.

To explore in detail the transition from nontopological (NS) to topological (TS) phases, we have observed the closing and reopening of the excitation gap $E_{\rm g}$, which is necessary to change the topology of the Fermi surface. In Fig. 6, we present a behavior of the order parameter $\Delta_{1,2} = \Delta$, the bulk quasiparticle gap $E_{\rm g}$, and the Chern number C while increasing the chemical potential μ and the interlayer phase φ. One can see that across the critical point where the Chern number changes abruptly, the excitation gap $E_{\rm g}$ vanishes, indicating the topological phase transition. The order parameter Δ increases with increasing chemical potential μ, and decreases with an increase of the interlayer phase φ with respect to $\pi/2$.

Finally, we show how the FFLO state evolves with increasing temperature in this bilayer system. Figure 7 gives BdG results for the density profiles, the phase configurations, as well as the momentum-space distributions of the order parameter for the first layer at different temperatures. (The order parameter looks similar in the second layer, so we have not displayed such plots.) With increasing temperature, the order parameter is destroyed gradually, and a large FFLO momentum $\approx(0.9\kappa, 0.9\kappa)$ is nearly independent of the temperature. In this case, it is much more difficult to disturb the FFLO state by thermal fluctuations compared to the TS phase. A further increase of the temperature will destroy the superfluid state eventually at around $T \approx 0.8T_F$.

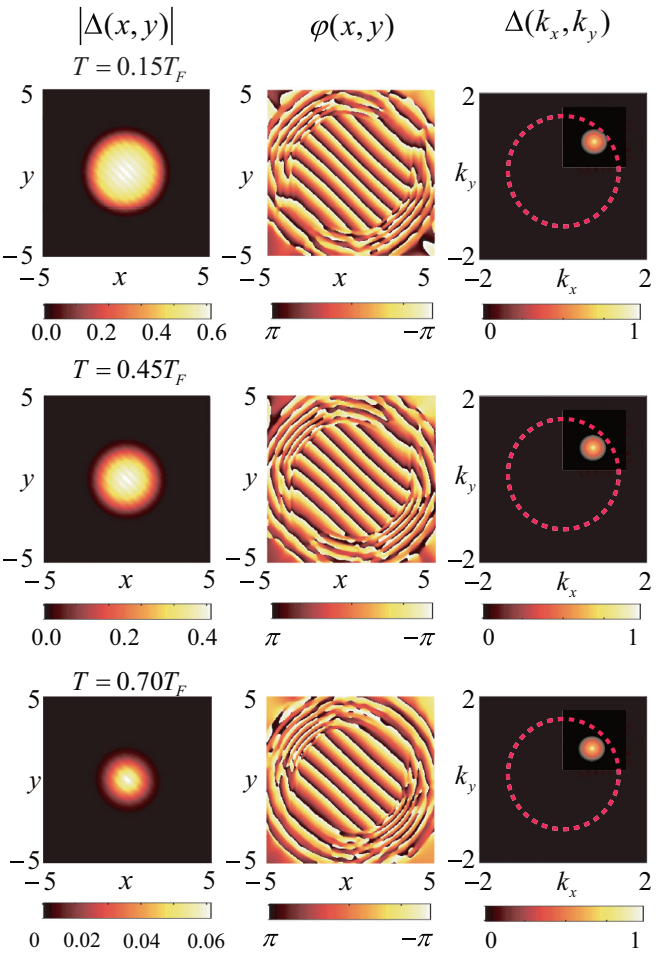

FIG. 7. Density profiles, phase configurations, and corresponding momentum-space distributions of the order parameter of the first layer at several temperatures: $T = 0.15T_F$ (upper panel), $T = 0.45T_F$ (middle panel), and $T = 0.7T_F$ (bottom panel). Other parameters are $\Omega = J = 0.4E_{\rm rec}$, $E_b = 1E_{\rm rec}$, $\varphi = 0.6\pi$, and $N_{\rm atom} = 100$. The characteristic temperature scale $T_F = E_F/k_B$ is given by the Fermi energy. The momentum is measured in the units of the recoil momentum κ.

IV. CONCLUDING REMARKS

We have investigated the superfluidity properties of a bilayer spin-orbit-coupled degenerate Fermi gas. The analysis has elucidated a diverse phase diagram of the bilayer superfluidity in a wide range of magnitudes of the atom-light coupling and atom-atom interaction. For the small to moderate atom-light coupling, the FFLO states occur. In the stronger coupling regime, the system undergoes a transition from the NS to TS phases. These effects can be experimentally detected for atomic fermions in a bilayer system. As discussed previously in the context of bosons [52], the bilayer scheme can be readily realized using three laser beams to induce the interlayer tunneling and the intralayer spin-flip transitions. In a similar manner, the bilayer scheme can be implemented for fermion atoms used in the previous experiments on the 1D SOC, such as ^{40}K [11].

ACKNOWLEDGMENTS

This work is supported by the NSFC under Grants No. 11474205, No. 11404225, and No.11504037, and the NKBRSFC under Grant No. 2012CB821305. G.J. acknowledges support by the Lithuanian Research Council (Grant No. MIP- 086/2015).

APPENDIX A: SINGLE-PARTICLE HAMILTONIAN

A single-particle part of the bilayer Hamiltonian (1) reads in the matrix representation

$$H_0 = \begin{pmatrix} \epsilon_{1\uparrow}(\mathbf{k}) & \Omega e^{-i\varphi} & J & 0 \\ \Omega e^{i\varphi} & \epsilon_{1\downarrow}(\mathbf{k}) & 0 & J \\ J^* & 0 & \epsilon_{2\uparrow}(\mathbf{k}) & \Omega e^{i\varphi} \\ 0 & J^* & \Omega e^{-i\varphi} & \epsilon_{2\downarrow}(\mathbf{k}) \end{pmatrix}, \tag{A1}$$

where the diagonal elements provide the SOC due to the recoil momentum $\sqrt{2}\kappa$:

$$\begin{aligned} \epsilon_{1\uparrow}(\mathbf{k}) &= \left[k_x^2 + (k_y - \kappa)^2\right]/2m - \mu, \\ \epsilon_{1\downarrow}(\mathbf{k}) &= \left[(k_x - \kappa)^2 + k_y^2\right]/2m - \mu, \\ \epsilon_{2\uparrow}(\mathbf{k}) &= \left[(k_x + \kappa)^2 + k_y^2\right]/2m - \mu, \\ \epsilon_{2\downarrow}(\mathbf{k}) &= \left[k_x^2 + (k_y + \kappa)^2\right]/2m - \mu. \end{aligned} \tag{A2}$$

Note that the Hamiltonian (A1) is related via a unitary transformation to the original Hamiltonian containing a position-dependent Raman coupling $\Omega e^{i[\kappa(x-y)\pm i\varphi]}$ and a position-dependent interlayer tunneling $Je^{i\kappa(x+y)}$ [52].

The Hamiltonian given by Eq. (A1) looks different from the one describing the SOC of the pure Rashba (or Dresselhaus) type. To establish a relation with the Rashba SOC, we set $\Omega = J$ and diagonalize the Hamiltonian (A1) for $k = 0$ via the following unitary transformation:

$$S = \frac{1}{2}\begin{pmatrix} -1 & \frac{1-e^{-i\varphi}}{\sqrt{2-2\cos(\varphi)}} & \frac{e^{-i\varphi}-1}{\sqrt{2-2\cos(\varphi)}} & 1 \\ 1 & \frac{1+e^{-i\varphi}}{\sqrt{2+2\cos(\varphi)}} & \frac{1+e^{-i\varphi}}{\sqrt{2+2\cos(\varphi)}} & 1 \\ -1 & \frac{e^{-i\varphi}-1}{\sqrt{2-2\cos(\varphi)}} & \frac{1-e^{-i\varphi}}{\sqrt{2-2\cos(\varphi)}} & 1 \\ 1 & -\frac{1+e^{-i\varphi}}{\sqrt{2+2\cos(\varphi)}} & -\frac{1+e^{-i\varphi}}{\sqrt{2+2\cos(\varphi)}} & 1 \end{pmatrix}. \tag{A3}$$

Thus one finds

$$\begin{aligned} H_{\rm SO} &= SH_0S^{-1} \\ &= \begin{pmatrix} \epsilon_{1+} & \alpha(k_y - ik_x) & 0 & \alpha(k_y + ik_x) \\ \alpha(k_y + ik_x) & \epsilon_{1-} & \alpha(k_y - ik_x) & 0 \\ 0 & \alpha(k_y + ik_x) & \epsilon_{2+} & \alpha(k_y - ik_x) \\ \alpha(k_y - ik_x) & 0 & \alpha(k_y + ik_x) & \epsilon_{2-} \end{pmatrix}, \end{aligned} \tag{A4}$$

where

$$\begin{aligned} \epsilon_{1+} &= \mathbf{k}^2/2m + E_{\rm rec} - \mu + 2\Omega\sin(\varphi/2), \\ \epsilon_{1-} &= \mathbf{k}^2/2m + E_{\rm rec} - \mu + 2\Omega\cos(\varphi/2), \\ \epsilon_{2+} &= \mathbf{k}^2/2m + E_{\rm rec} - \mu - 2\Omega\sin(\varphi/2), \\ \epsilon_{2-} &= \mathbf{k}^2/2m + E_{\rm rec} - \mu - 2\Omega\cos(\varphi/2), \end{aligned} \tag{A5}$$

and $\alpha = \kappa/2m$.

By tuning the strength Ω and the phase difference φ of the Raman coupling, one can reach a regime where $2\Omega\sin(\varphi/2) \gg E_{\rm rec}$ and $\sin(\varphi/2) \approx \cos(\varphi/2)$, so $\varphi \approx \pi/2$. Under these conditions the low-energy physics is described by the two lowest energy branches $\epsilon_{2\pm}$ characterized by the eigenvectors $|2\pm\rangle$. Neglecting the upper two dispersion branches $\epsilon_{1\pm}$ separated from $\epsilon_{2\pm}$ by approximately 4Ω, one arrives at an effective low-energy 2×2 matrix Hamiltonian:

$$H_{\rm eff} = \begin{pmatrix} \mathbf{k}^2/2m - \mu' - h_z & \alpha(k_y - ik_x) \\ \alpha(k_y + ik_x) & \mathbf{k}^2/2m - \mu' + h_z \end{pmatrix}, \quad \text{(A6)}$$

where h_z is an effective Zeeman term generated by a slight change of the phase around $\varphi = \pi/2$ [45]:

$$h_z = \Omega[\sin(\varphi/2) - \cos(\varphi/2)] = \Omega\sqrt{2}\sin(\delta\varphi/2), \quad \text{(A7)}$$

with $\delta\varphi = \varphi - \pi/2$. Here $\mu' = \mu - \Delta\mu$ is an effective chemical potential with $\Delta\mu = E_{\rm rec} - \Omega[\sin(\varphi/2) + \cos(\varphi/2)]$.

The Hamiltonian (A6) can be cast in terms of the unit 2×2 matrix I and three Pauli matrices $\sigma_{x,y,z}$:

$$H_{\rm eff} = (\mathbf{k}^2/2m - \mu')I + \alpha(k_x\sigma_y + k_y\sigma_x) + h_z\sigma_z. \quad \text{(A8)}$$

The SOC term $k_x\sigma_y + k_y\sigma_x$ is equivalent to the Rashba SOC term $-k_x\sigma_y + k_y\sigma_x$ after interchanging the dressed states $|2+\rangle \leftrightarrow |2-\rangle$. In fact, such an interchange leads to $\sigma_y \to -\sigma_y$ and $\sigma_{x,z} \to \sigma_{x,z}$.

Unlike in the previous study on the bilayer bosons [52], we do not take the phase φ to be $\pi/2$ in the effective Hamiltonian $H_{\rm eff}$. This allows one to include the Zeeman term playing an important role in the topological superfluidity.

APPENDIX B: CALCULATION OF THE CHERN NUMBER

To calculate the Chern number, we assume that the whole region is homogenous for a sufficiently weak harmonic trap, and transform the BdG Hamiltonian to the momentum space, $H = \sum_{\mathbf{k}} \frac{1}{2}\phi^\dagger_{\mathbf{k}} H_{\rm BdG}(\mathbf{k})\phi_{\mathbf{k}}$, where

$$H_{\rm BdG}(\mathbf{k}) = \begin{pmatrix} H_1(\mathbf{k}) & \mathcal{J} \\ \mathcal{J}^\dagger & H_2(\mathbf{k}) \end{pmatrix}, \quad \text{(B1)}$$

with

$$H_1(\mathbf{k}) = \begin{pmatrix} \epsilon_{1\uparrow}(\mathbf{k}) & \Omega e^{-i\varphi} & 0 & \Delta_1 \\ \Omega e^{i\varphi} & \epsilon_{1\downarrow}(\mathbf{k}) & -\Delta_1 & 0 \\ 0 & -\Delta_1^* & -\epsilon_{1\uparrow}(-\mathbf{k}) & -\Omega e^{-i\varphi} \\ \Delta_1^* & 0 & -\Omega e^{i\varphi} & -\epsilon_{1\downarrow}(-\mathbf{k}) \end{pmatrix}, \quad \text{(B2)}$$

and

$$H_2(\mathbf{k}) = \begin{pmatrix} \epsilon_{2\uparrow}(\mathbf{k}) & \Omega e^{i\varphi} & 0 & \Delta_2 \\ \Omega e^{-i\varphi} & \epsilon_{2\downarrow}(\mathbf{k}) & -\Delta_2 & 0 \\ 0 & -\Delta_2^* & -\epsilon_{2\uparrow}(-\mathbf{k}) & -\Omega e^{i\varphi} \\ \Delta_2^* & 0 & -\Omega e^{-i\varphi} & -\epsilon_{2\downarrow}(-\mathbf{k}) \end{pmatrix}. \quad \text{(B3)}$$

Here we have chosen the Nambu basis $\phi_{\mathbf{k}} = [c_{1\uparrow,\mathbf{k}}, c_{1\downarrow,\mathbf{k}}, c^\dagger_{1\uparrow,-\mathbf{k}}, c^\dagger_{1\downarrow,-\mathbf{k}}, c_{2\uparrow,\mathbf{k}}, c_{2\downarrow,\mathbf{k}}, c^\dagger_{2\uparrow,-\mathbf{k}}, c^\dagger_{2\downarrow,-\mathbf{k}}]^T$. To determine the topological character, we then proceed to calculate the Chern number $C = 1/2\pi \int d\mathbf{k}^2\Omega(\mathbf{k})$, where the $\Omega(\mathbf{k})$ is the usual Berry curvature for the momentum states [75]

$$\Omega(\mathbf{k}) = -2\sum_n \sum_{m\neq n} f_n \times \mathrm{Im}\frac{\langle\psi_n(\mathbf{k})|v_{k_x}|\psi_m(\mathbf{k})\rangle\langle\psi_m(\mathbf{k})|v_{k_y}|\psi_n(\mathbf{k})\rangle}{[\varepsilon_m(\mathbf{k}) - \varepsilon_n(\mathbf{k})]^2}. \quad \text{(B4)}$$

Here $f_n = 1/[e^{\varepsilon_n/k_BT} + 1]$ is the Fermi-Dirac distribution function, a subscript n ($n = 1,2,\ldots,8$) labels all eight particle-hole bands of the momentum-space BdG Hamiltonian, and $\psi_n(\mathbf{k})$ is a wave function of eigenenergy $\varepsilon_n(\mathbf{k})$, with v_{k_x} and v_{k_y} being velocity operators.

In Fig. 5 the order parameter and the chemical potential are given by the self-consistent solution of the BdG equation (8) at the center of the trap where the changes in the trapping potential are minimum. For the NS and TS phases the order parameter is constant, so the momentum representation is relevant.

[1] M. Z. Hasan and C. L. Kane, Rev. Mod. Phys. **82**, 3045 (2010).
[2] X. L. Qi and S. C. Zhang, Rev. Mod. Phys. **83**, 1057 (2011).
[3] M. Lewenstein, A. Sanpera, V. Ahufinger, B. Damski, A. Sen (De), and U. Sen, Adv. Phys. **56**, 243 (2007).
[4] I. Bloch, J. Dalibard, and W. Zwerger, Rev. Mod. Phys. **80**, 885 (2008).
[5] J. Dalibard, F. Gerbier, G. Juzeliūnas, and P. Öhberg, Rev. Mod. Phys. **83**, 1523 (2011).
[6] M. Lewenstein, A. Sanpera, and V. Ahufinge, *Ultracold Atoms in Optical Lattices: Simulating Quantum Many-Body Systems* (Oxford University, Oxford, 2012).
[7] N. Goldman, G. Juzeliūnas, P. Öhberg, and I. B. Spielman, Rep. Prog. Phys. **77**, 126401 (2014).
[8] N. Goldman, J. C. Budich, and P. Zoller, Nat. Phys. **12**, 639 (2016).
[9] Y.-J. Lin, K. Jiménez-García, and I. B. Spielman, Nature (London) **471**, 83 (2011).
[10] J.-Y. Zhang, S.-C. Ji, Z. Chen, L. Zhang, Z.-D. Du, B. Yan, G.-S. Pan, B. Zhao, Y.-J. Deng, H. Zhai, S. Chen, and J.-W. Pan, Phys. Rev. Lett. **109**, 115301 (2012).
[11] P. J. Wang, Z.-Q. Yu, Z. K. Fu, J. Miao, L. H. Huang, S. J. Chai, H. Zhai, and J. Zhang, Phys. Rev. Lett. **109**, 095301 (2012).
[12] L. W. Cheuk, A. T. Sommer, Z. Hadzibabic, T. Yefsah, W. S. Bakr, and M. W. Zwierlein, Phys. Rev. Lett. **109**, 095302 (2012).
[13] C. Qu, C. Hamner, M. Gong, C. W. Zhang, and P. Engels, Phys. Rev. A **88**, 021604(R) (2013).
[14] L. Huang, Z. Meng, P. Wang, P. Peng, S.-L. Zhang, L. Chen, D. Li, Q. Zhou, and J. Zhang, Nat. Phys. **12**, 540 (2016).
[15] Z. Meng, L. Huang, P. Peng, D. Li, L. Chen, Y. Xu, C. Zhang, P. Wang, and J. Zhang, Phys. Rev. Lett. **117**, 235304 (2016).
[16] Z. Wu, L. Zhang, W. Sun, X.-T. Xu, B.-Z. Wang, S.-C. Ji, Y. Deng, S. Chen, X.-J. Liu, and J.-W. Pan, Science **354**, 83 (2016).

[17] J. Li, W. Huang, B. Shteynas, S. Burchesky, F. C. Top, E. Su, J. Lee, A. O. Jamison, and W. Ketterle, Phys. Rev. Lett. **117**, 185301 (2016).
[18] H. Zhai, Int. J. Mod. Phys. B **26**, 1230001 (2013).
[19] V. Galitski and I. B. Spielman, Nature **494**, 49 (2013).
[20] C. J. Wang, C. Gao, C.-M. Jian, and H. Zhai, Phys. Rev. Lett. **105**, 160403 (2010).
[21] T.-L. Ho and S. Z. Zhang, Phys. Rev. Lett. **107**, 150403 (2011).
[22] Z. F. Xu, R. Lü, and L. You, Phys. Rev. A **83**, 053602 (2011).
[23] Y. P. Zhang, L. Mao, and C. W. Zhang, Phys. Rev. Lett. **108**, 035302 (2012).
[24] Y. Li, L. P. Pitaevskii, and S. Stringari, Phys. Rev. Lett. **108**, 225301 (2012).
[25] J. P. Vyasanakere, S. Zhang, and V. B. Shenoy, Phys. Rev. B **84**, 014512 (2011).
[26] S. Sinha, R. Nath, and L. Santos, Phys. Rev. Lett. **107**, 270401 (2011).
[27] T. Kawakami, T. Mizushima, M. Nitta, and K. Machida, Phys. Rev. Lett. **109**, 015301 (2012).
[28] H. Hu, B. Ramachandhran, H. Pu, and X.-J. Liu, Phys. Rev. Lett. **108**, 010402 (2012).
[29] R. M. Wilson, B. M. Anderson, and C. W. Clark, Phys. Rev. Lett. **111**, 185303 (2013).
[30] W. Han, G. Juzeliúnas, W. Zhang, and W.-M. Liu, Phys. Rev. A **91**, 013607 (2015).
[31] Q. Sun, J. Hu, W. Lin, W.-M. Liu, G. Juzeliúnas, and A.-C. Ji, Sci. Rep. **6**, 37679 (2016).
[32] L. Jiang, X.-J. Liu, H. Hu, and H. Pu, Phys. Rev. A **84**, 063618 (2011).
[33] J. P. Vyasanakere and V. B. Shenoy, New J. Phys. **14**, 043041 (2012).
[34] H. Hu, L. Jiang, X.-J. Liu, and H. Pu, Phys. Rev. Lett. **107**, 195304 (2011).
[35] M. Gong, S. Tewari, and C. W. Zhang, Phys. Rev. Lett. **107**, 195303 (2011).
[36] Z.-Q. Yu and H. Zhai, Phys. Rev. Lett. **107**, 195305 (2011).
[37] M. Gong, G. Chen, S.-T. Jia, and C. W. Zhang, Phys. Rev. Lett. **109**, 105302 (2012).
[38] L. Dong, L. Jiang, and H. Pu, New J. Phys. **15**, 075014 (2013).
[39] J. Ruseckas, G. Juzeliūnas, P. Öhberg, and M. Fleischhauer, Phys. Rev. Lett. **95**, 010404 (2005).
[40] T. D. Stanescu, C. Zhang, and V. Galitski, Phys. Rev. Lett. **99**, 110403 (2007).
[41] A. Jacob, P. Öhberg, G. Juzeliūnas, and L. Santos, Appl. Phys. B **89**, 439 (2007).
[42] G. Juzeliūnas, J. Ruseckas, M. Lindberg, L. Santos, and P. Öhberg, Phys. Rev. A **77**, 011802(R) (2008).
[43] T. D. Stanescu, B. Anderson, and V. Galitski, Phys. Rev. A **78**, 023616 (2008).
[44] G. Juzeliūnas, J. Ruseckas, and J. Dalibard, Phys. Rev. A **81**, 053403 (2010).
[45] D. L. Campbell, G. Juzeliūnas, and I. B. Spielman, Phys. Rev. A **84**, 025602 (2011).
[46] Z. F. Xu and L. You, Phys. Rev. A **85**, 043605 (2012).
[47] B. M. Anderson, G. Juzeliūnas, V. M. Galitski, and I. B. Spielman, Phys. Rev. Lett. **108**, 235301 (2012).
[48] B. M. Anderson, I. B. Spielman, and G. Juzeliūnas, Phys. Rev. Lett. **111**, 125301 (2013).
[49] Z.-F. Xu, L. You, and M. Ueda, Phys. Rev. A **87**, 063634 (2013).
[50] X.-J. Liu, K. T. Law, and T. K. Ng, Rev. Lett. **112**, 086401 (2014).
[51] Q. Sun, L. Wen, W.-M. Liu, G. Juzeliūnas, and A.-C. Ji, Phys. Rev. A **91**, 033619 (2015).
[52] S.-W. Su, S.-C. Gou, Q. Sun, L. Wen, W.-M. Liu, A.-C. Ji, J. Ruseckas, and G. Juzeliūnas, Phys. Rev. A **93**, 053630 (2016).
[53] D. Jaksch and P. Zoller, New J. Phys. **5**, 56 (2003).
[54] M. Aidelsburger, M. Atala, S. Nascimbène, S. Trotzky, Y. A. Chen, and I. Bloch, Phys. Rev. Lett. **107**, 255301 (2011).
[55] M. Aidelsburger, M. Atala, M. Lohse, J. T. Barreiro, B. Paredes, and I. Bloch, Phys. Rev. Lett. **111**, 185301 (2013).
[56] H. Miyake, G. A. Siviloglou, C. J. Kennedy, W. C. Burton, and W. Ketterle, Phys. Rev. Lett. **111**, 185302 (2013).
[57] M. Atala, M. Aidelsburger, M. Lohse, J. T. Barreiro, B. Paredes, and I. Bloch, Nat. Phys. **10**, 588 (2014).
[58] C. Zhang, S. Tewari, R. M. Lutchyn, and S. Das Sarma, Phys. Rev. Lett. **101**, 160401 (2008).
[59] M. Sato, Y. Takahashi, and S. Fujimoto, Phys. Rev. Lett. **103**, 020401 (2009).
[60] X.-L. Qi, T. L. Hughes, S. Raghu, and S.-C. Zhang, Phys. Rev. Lett. **102**, 187001 (2009).
[61] Y. Xu, L. Mao, B. Wu, and C. Zhang, Phys. Rev. Lett. **113**, 130404 (2014).
[62] J.-H. Zheng, D.-W. Wang, and G. Juzeliūnas, Sci. Rep. **6**, 33320 (2016).
[63] B. Xiong, J.-H. Zheng, Y.-J. Lin, and D.-W. Wang, Phys. Rev. A **94**, 063611 (2016).
[64] Y.-A. Liao, A. Rittner, T. Paprotta, W. Li, G. Partridge, R. Hulet, S. Baur, and E. Mueller, Nature **467**, 567 (2010).
[65] H. Hu and X.-J. Liu, Phys. Rev. A **73**, 051603(R) (2006).
[66] M. Iskin and A. L. Subasi, Phys. Rev. A **87**, 063627 (2013).
[67] C. Qu, Z. Zheng, M. Gong, Y. Xu, L. Mao, X. Zou, G. Guo, and C. Zhang, Nat. Commun. **4**, 2710 (2013).
[68] W. Zhang and W. Yi, Nat. Commun. **4**, 2711 (2013).
[69] V. V. França, D. Hörndlein, and A. Buchleitner, Phys. Rev. A **86**, 033622 (2012).
[70] J. Sebby-Strabley, M. Anderlini, P. S. Jessen, and J. V. Porto, Phys. Rev. A **73**, 033605 (2006).
[71] For more details see Appendix A, as well as Appendix A of Ref. [52].
[72] M. Randeria, J.-M. Duan, and L.-Y. Shieh, Phys. Rev. Lett. **62**, 981 (1989).
[73] P. G. de Gennes, *Superconductivity of Metals and Alloys* (Westview, New York, 1999).
[74] R. Onofrio, Usp. Fiz. Nauk **186**, 1229 (2016).
[75] D. Xiao, M.-C. Chang, and Q. Niu, Rev. Mod. Phys. **82**, 1959 (2010).